Visualization Experiments of Radiation Heating on the Eutectic Reaction between B_4C-SS and Its Relocation Behavior

Zeeshan Ahmed[a], Avadhesh Kumar Sharma[a], Marco Pellegrini[a], Hidemasa Yamano[b], Koji Okamoto[a]*

[a] Department of Nuclear Engineering and Management, The University of Tokyo, 7-3-1 Hongo, Bunkyo, Tokyo, 113-8656, Japan
[b] *Japan Atomic Energy Agency (JAEA), 4002 Narita-cho, Oarai, Ibaraki, 311-1393, Japan*

**E-mail: ahmed14310024@gmail.com*

Abstract – *The development of Generation IV Sodium-cooled Fast Reactors (SFRs) faces a crucial challenge concerning Core Disruptive Accidents (CDAs). The eutectic reaction between boron carbide (B_4C) and Stainless Steel (SS) can lead to boron migration, resulting in the formation of a molten pool that may relocate extensively within the core, thereby affecting neutron balance in the disrupted core. To address this in CDA analyses, in this study, the eutectic behavior and subsequent melt structure of boron migration are observed by a quantitative and high-resolution visualization method using radiative heating. Experiments were conducted using B_4C pellet and powder within SS tubes, replicating the actual control rod design in the temperature range of 1150 °C to 1372 °C to study long-duration melting and relocation behavior, which has not been done before. The study observed that the eutectic temperature for the pellet case was higher than the powder case and was not influenced by the heating rate. Two failure mechanisms were observed: firstly, the SS peeling off the B_4C pellet and powder, subsequently coalescing into a molten droplet; secondly, the B_4C pellet breaking into multiple pieces due to thermal stress, along with sintering observed in the B_4C powder case. The visualization technique accurately identified the time of eutectic melting onset and the related temperature, pointing out different values for the pellet and the powder cases. This study offers valuable insights into the relocation behavior of the eutectic melt, aiding in understanding the eutectic reaction mechanism in control rods and contributing to ensuring the safety of CDAs in SFRs.*

Keywords: B_4C, Stainless Steel-304 (SS), Eutectic melting, Radiative heating visualization, Sodium-cooled fast reactor

I. Introduction

A sodium-cooled fast reactor (SFR) is a Generation IV reactor designed to improve reliability, safety, and economic efficiency. However, a significant challenge in SFR development is the potential occurrence of a core disruptive accident (CDA). An in-vessel retention strategy has been adopted to keep degraded core materials cooled within the reactor vessel in Japan **[1].** The Japan Atomic Energy Agency (JAEA) has been investigating this scenario using experiments and numerical analyses **[2,3].** In the past, a CDA scenario was postulated to study the progression of events, especially during the material relocation and heat-removal phases **[4].** The concern during a CDA in SFRs is the eutectic reaction between B_4C pellets and SS cladding, where studying B_4C ingress into the degraded core becomes essential to mitigate recriticality risks during the relocation phase, given its strong neutron absorbing properties, and particularly since the eutectic temperature (1230 ºC) is lower than the individual melting points of B_4C (2500 ºC) and SS (1400 ºC) **[5,6].** This reaction causes the melted debris to disperse throughout the core, changing the neutron balance in the disrupted core, particularly during the relocation phase**.** To ensure the safety assessment of CDAs in SFRs, it is crucial to fully understand the

eutectic reaction mechanism and the behavior of the resulting melt debris during relocation through visualization.

There are two main methods for visualizing melt behavior: time-resolved and static. Previous studies on the eutectic reaction between B_4C and SS have primarily used static methods to observe the chemical interaction and melt initiation after annealing tests [**7-10**]. However, dynamic visualization has been limited due to challenges posed by the high eutectic temperature and the coexistence of solids and liquids during the phenomenon. These factors make dynamic visualization difficult, as the thermal expansion and deformation of the specimen and apparatus can lead to mechanical failure, and heater-emitted solid light can disturb clear visualization. Various time-resolved visualization methods have been developed for other applications, including radioscopic methods **[11]**, dynamic neutron computer tomography **[12]**, and ultrasonic visualization **[13-14]**. However, these methods are not well-suited for scenarios where solids and liquids coexist during the phenomenon, and their interaction is crucial.

Additionally, they do not consider high temperatures. Some methods for in-situ visualization of phase transformations at high temperatures have been developed, such as high-temperature laser microscopy **[9,15]** and a high-speed video camera **[16]**. Nevertheless, these approaches have limitations, such as a small specimen scale and an inability to observe the entire process, from melt growth to melt flow, in a time sequence. Ueda et al. **[17]** conducted a study in which they performed time-resolved visualization of the eutectic reaction between boron carbide powder and stainless steel at temperatures up to 1250 ºC. They observed that the specimen's geometry changes affected the melting behavior during the eutectic reaction. Yamano et al. **[18]** also described basic experiments to visualize the reaction of a B_4C block contacted with molten SS in a high-temperature heating furnace. Their experiments indicated that the eutectic reaction and solidification of the B_4C-SS eutectic occurred in the upper part of the solidified test section, separated from the solidified SS due to the density difference.

Previous studies have not utilized the actual control rod material and design, which consists of B_4C material with SS cladding, in radiation experiments to investigate the eutectic onset. This limitation raises concerns about accurately representing the behavior of the control rod under operational conditions in SFRs. As a result, there is a pressing need for a new and straightforward visualization technique that can effectively capture both melt growth and melt behavior in a time sequence at high temperatures. This would enable dynamic visualization of the eutectic reaction in real control rods. Developing such a visualization experiment with well-defined boundary conditions can gain essential insights into the eutectic reaction mechanism. Additionally, the experimental data obtained from this novel visualization approach can serve as valuable validation data for numerical calculations of the phenomena. This will contribute to a better understanding of the eutectic reaction in control rods and enhance the safety assessment of CDAs in SFRs.

In this study, we conducted visualization experiments on the B_4C-SS eutectic reaction using a cylindrical control rod with B_4C as the pellet and powder enclosed within full and half SS pipes. For the first time, we observed the long-duration melting behavior of the eutectic melt and its relocation behavior. To ensure clear visualization, we successfully employed radiative heating, overcoming challenges like thermal expansion, reflected light, and changes in specimen geometry. Our experiments at different temperatures and with various specimens validated the technique's effectiveness, with clear images obtained up to 1372 °C. The technique effectively captured dynamic phenomena and geometrical information at high temperatures, making it a potential tool for validating numerical simulations. Notably, our long-duration heating approach allowed us to study the entire relocation process, which is impossible in Joule heating experiments **[19]**. These findings hold significant implications for understanding the B_4C-SS eutectic reaction's behavior under high-temperature conditions, contributing valuable insights to developing more efficient and safer SFRs.

II. Eutectic relocation experiment using a radiating heating test facility

II.A. Heating Method

The chosen heating method for the high-temperature eutectic reaction visualization should meet specific criteria: reaching temperatures up to 1372 °C, enabling non-contact heating for undisturbed melt movement observation, and allowing long-term melting without introducing additional chemicals. Radiative heating using tungsten heaters fulfils these requirements. It

offers advantages like clear visualization without enclosing the specimen, fixed boundary conditions for post-analysis, and consistent heat flux throughout the process. However, radiative heating emits intense light at high temperatures, which can interfere with the visualization camera. To address this, optical tools are utilized to minimize the impact of light interference.

II.B. Materials

Figure 1 provides a top-view schematic of the specimens' design and the tungsten heaters used in the radiation heating experiments. The specimen comprises a cylindrical B_4C pellet and powder within a SUS304 (SS) half/full tube. The pellet has dimensions of 20mm in diameter and 45mm in height, while the powder size is approximately 30-35 µm calculated using ImageJ **[20]** and scanning electron microscopy (SEM), as shown in Figure 2.

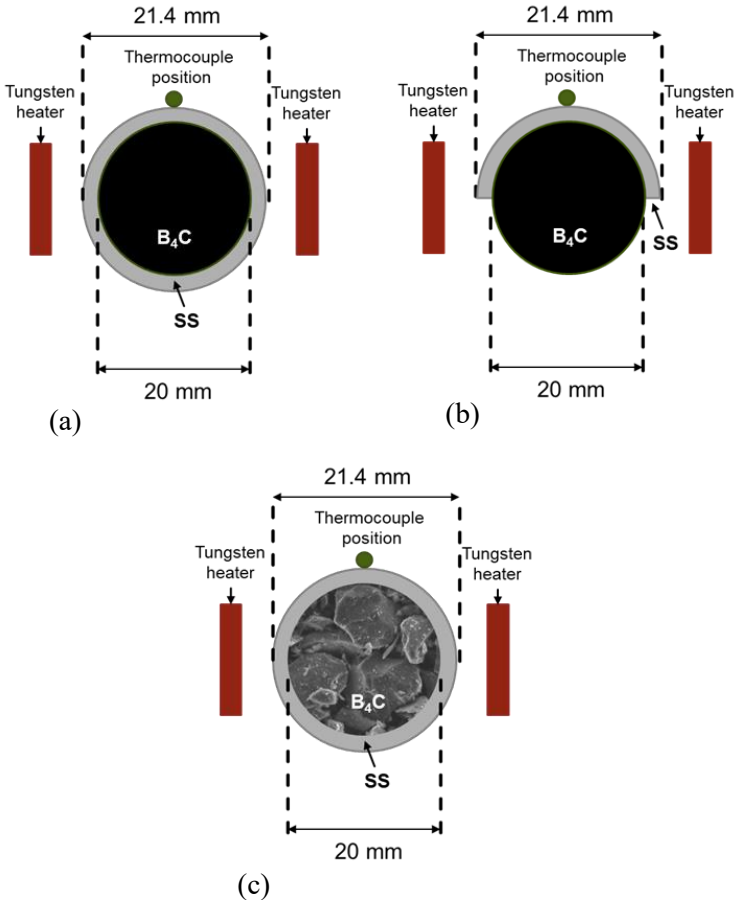

Fig. 1. Specimens designed to perform experiments (a) Full SS+ B_4C pellet, (b) Half SS+ B_4C pellet, and (c) Full SS+ B_4C powder

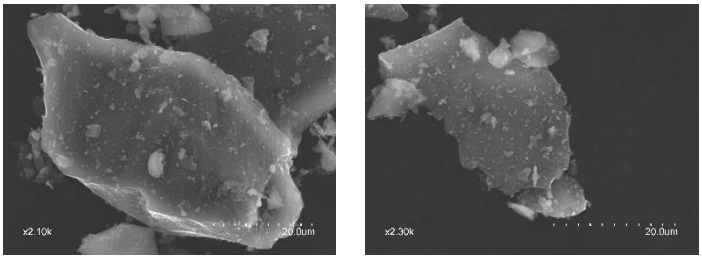

(a) (b)

Fig. 2. SEM images of powder to determine its size

The SS cylinder consists of a lower section, a full cylinder with an external diameter of 25.4mm and a height of 10mm, supporting the pellet and collecting the solidified melt. The upper section is a half-cylinder cut along the axis, with an outer diameter of 21.4mm and a height of 45mm. Using a high-speed camera, the goal is to observe the eutectic reaction progress at the B_4C-SS interface. Both the half and full cylinders have an internal diameter of 20.2mm. Three scenarios are tested to enable comparative analysis of the eutectic melting and relocation behavior: Half SS+ B_4C pellet, Full SS+ B_4C pellet, and Full SS+ B_4C powder. This involves using SS full tubes, half tubes with the exact dimensions, the B_4C pellet, and SS full tubes with B_4C powder. The tungsten heaters used in the experiment are thin sheets with a thickness of 0.5mm and a length of 90mm. The top and bottom ends of the heaters are wider for secure fixation, while the middle section, with a width of 12 mm, serves as the heating element, generating the required heat flux for the specimen.

II.C. Experimental facility

Figure 3 depicts the developed system for visualization of the eutectic melting progress using tungsten heaters positioned beside the B_4C -SS sample for controlled heating. The sample is placed between the tungsten heaters, which are heated to high temperatures via the current application, and the sample is heated through radiation. However, the thermal expansion of tungsten heaters at high temperatures proved significant, reaching an estimated temperature exceeding 3000 °C, while the desired specimen temperature was only above 1372 °C. This caused continuous expansion, deformation, and eventual contact with the specimen, leading to an electric short circuit. To address this issue, a traction device with a weight and bearing mechanism was utilized to exert a downward pull on the heaters, releasing stress and preventing

deformation. Copper electrodes connected to the power supply enabled the heating process. To monitor and record crucial data like temperature, pressure, voltage, and current signals, K-type thermocouples were affixed to the outer surfaces of the SS component. A data logger continuously collected this information. Cooling fins were strategically placed near the sample region to transfer excess heat to the atmosphere, helping to regulate the temperature. An observation window was positioned in front of the facility to allow clear visualization using a high-speed camera (FASTCAM SA-X, Photron Co.). To prevent reflections from direct light emitted by the tungsten heaters, a slit was incorporated into the observation window. A neutral density filter was also placed on the camera to reduce surplus light uniformly. The gas inlet and outlet were located at the back of the test facility to maintain the required Argon atmosphere.

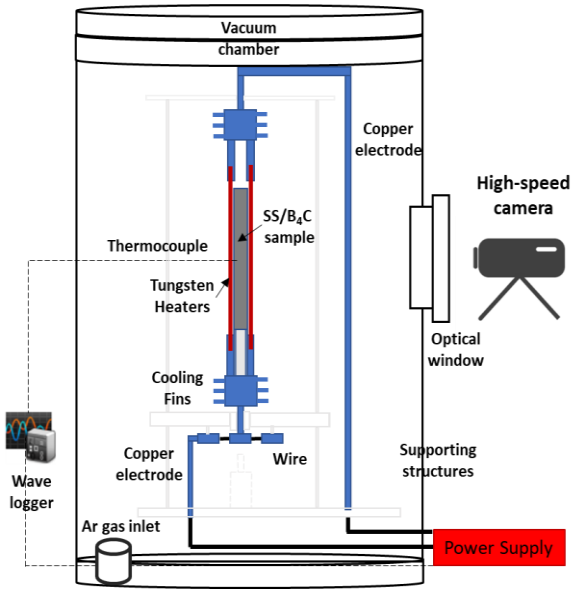

Fig .3. A schematic image of the test facility

II.D. Experimental methodology

In the current experimental setup, all three combinations of B_4C -SS specimens are positioned on a copper base with the assistance of an SS holder to ensure stability. To achieve uniform heating from the tungsten heaters, the copper shaft is carefully smoothened, and a frictionless arrangement is designed to prevent any bending of the heaters. To prevent oxidation of the tungsten heaters at high temperatures, a vacuum chamber depicted in schematic figure 3 is utilized. A vacuum pump creates a perfect vacuum condition at -101.5 kPa pressure. After depressurization, the chamber is filled with Argon gas to create an inert atmosphere. Once the system is fully covered, Argon gas is introduced to maintain the inert atmosphere during the experiment, and the experiments are conducted under Argon pressure conditions (101.5 kPa). The high-speed camera is positioned before the observation window for clear visualization. The radiation heating experiment begins by gradually increasing the current in incremental steps until the voltage signal reaches its maximum limit (10V DC source). Two different heating rates are applied, 0.45 ºC/s and 0.3 ºC/s, to observe the effect of heating rate on eutectic temperature. The high-speed camera records the video to observe long-duration radiative heating while the system operates up to the maximum constant power ($P_{max}=V_{max}*I_{max}$). Throughout the experiment, a data logger continuously records voltage, current, and temperature measurements at the interface and centre of the specimen, as shown in Figure 3. This comprehensive data collection enables precise analysis and observation of the eutectic reaction process.

III. Results and Discussions

III.A. Visualization of Eutectic reaction and liquefication process

(1) B_4C pellet with full and half SS pipe

To examine the eutectic melting between the B_4C pellet and SS, the pellet is placed inside the SS tube with a 0.1 mm clearance between them. To avoid premature breakage due to prolonged exposure to the Tungsten heater, the thermocouple was not positioned directly at the SS surface facing the heater. The experiments revealed that eutectic melting began when the measured external cladding temperature ranges from 1300-1310 ºC, as shown in Figure 4, with an approximate power of up to 10000 W. The maximum temperature achieved by the specimen depended on the heating rate and the distance from the Tungsten heaters. This variability was evident in the test results shown in Figure 4, where two different heating rates were employed for each specimen's design, as discussed in section *II.D*. However, it is essential to emphasize that the eutectic onset consistently occurred within the specified temperature range in repeatable experiments. This consistency was deemed more critical than the heating rate. Since one of the study's

objectives was to observe the long-term behavior of eutectic melting and its relocation, we continued the experiment by increasing the Tungsten power to understand the behavior of the melt formed. The highest temperature recorded was 1372 ºC, limited by the K-type thermocouple. The formed mixture of B_4C and SS undergoes melting due to diffusion of atoms. Subsequently, it descends primarily under the influence of gravity. However, viscosity and surface tension affect the flow and mixing of the molten B_4C-SS mixture, along with diffusion and gravity influencing its movement. According to Babar et al. **[21]**, the liquefied eutectic material had a low viscosity of approximately 1.0–20 mPa·s, which could be one of the contributing factors. Nagase et al.'s **[8]** investigation show that the eutectic melt invasion was not observed in the study while taking a pellet case which does not align with our current work as low surface tension in our experiment during long-term heating results in the downward movement and flow of the eutectic melt.

During the eutectic melting, the pellets were observed to fracture into several fragments possibly due to radial and thermal stresses developed within the pellet due to radiation heating. This phenomenon is observed in half and full SS cases and is the inevitable consequence of the temperature gradients across the pellet. Moreover, two distinct mechanisms were identified during the extended heating of the eutectic melt. The first mechanism entailed the separation of the stainless-steel layer, followed by creation of a molten drop containing both B_4C and stainless steel, which would subsequently migrate to the bottom of the specimen. Then the melt relocated at the bottom after receiving long-term heat, which reduced the viscosity and surface tension and reached the bottom where it is exposed to the bottom surface of the heater where the temperature is much lower than the middle portion. Hence, the eutectic melt becomes more viscous at this position and does not move further and solidify after 3000s once the experiment was stopped near the SS bottom support. When boron carbide and stainless steel are in contact, the diffusion process is influenced by their distinct material properties. In the B_4C pellet and SS full pipe configuration, we observed a smooth peeling-off mechanism of SS over the pellet surface. This can be attributed to the diffusion phenomenon occurring between the B_4C pellet and SS interface. The B_4C material is compact and dense in pellet case, allowing for a larger contact area and more direct interaction with SS. The crystal structure of B_4C in the pellet configuration facilitates a better match with the SS lattice, promoting the movement of atoms across the interface. As the temperature increases, the enhanced diffusion and solid-solid interaction between B_4C and SS lead to a smoother and more complete peeling-off of the SS layer from the B_4C pellet surface when subjected to external heating. The bonding between B_4C and SS weakens significantly, causing the SS layer to detach more effectively. However, the peeling-off mechanism in the half SS tube case is not that smooth due to the absence of SS atoms in the circumferential direction. Hence, even after eutectic melting, the SS layer experiences partial separation from the B_4C pellet.

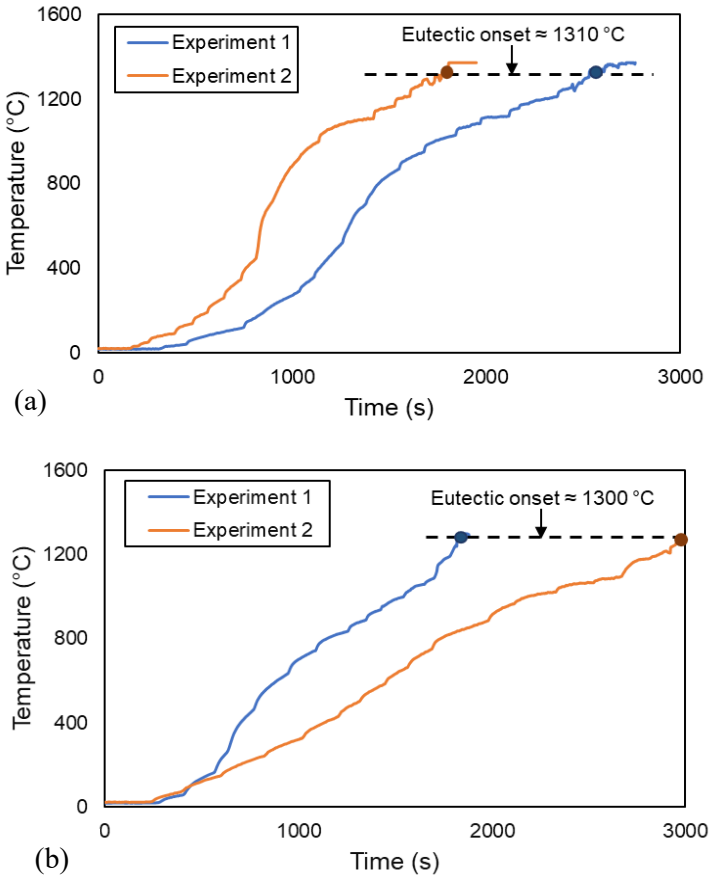

Fig. 4. (a) shows B_4C -Half SS pipe and (b) shows B_4C-Full SS pipe temperature profile with eutectic onset in two experiments with different heating rates.

One must note that the half SS tubes provided a more transparent and detailed view of the interface region where the eutectic melt occurs, as the interface is exposed and visible. There is no limitation to the viewing area, as shown in Figures 5 (a) and (b). On the

other hand, full tubes were used to observe the mechanisms involved in the eutectic melting after initiating it. Figures 6 (a) and 6 (b) show the visualization test results taken by the high-speed camera for the full tube pellet case.

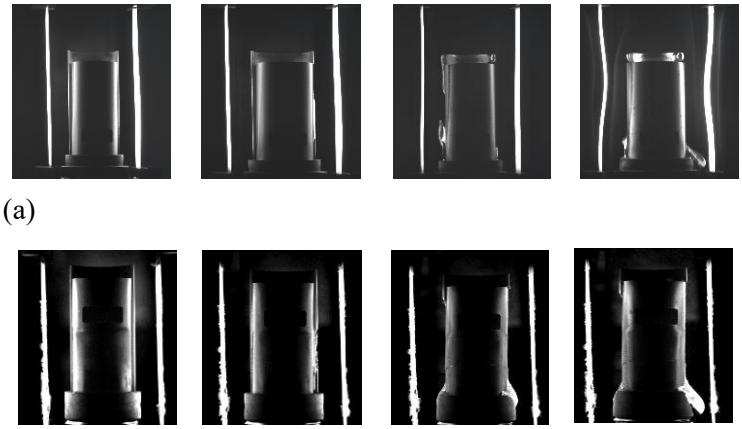

Fig. 5. (a) Experiment 1 and (b) Experiment 2 show the pictorial representation of the half SS pipe-pellet case from the start of the eutectic reaction to melt formation.

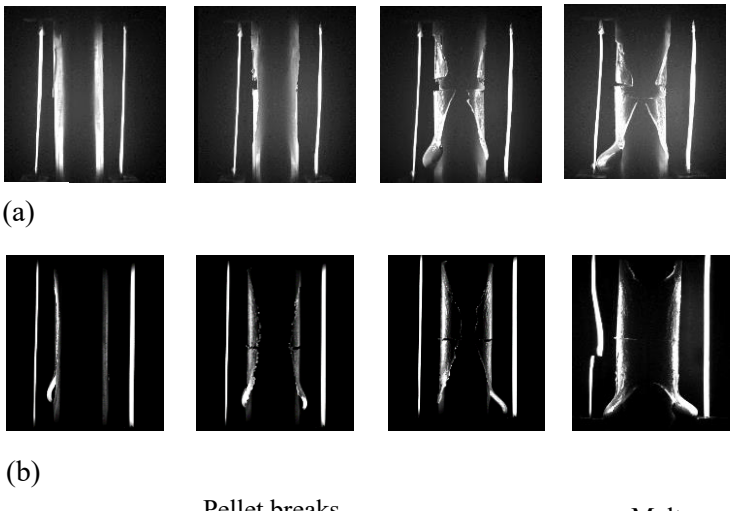

Fig. 6. (a) Experiment 1 and (b) Experiment 2 show the pictorial representation of the full SS pipe-pellet case from the start of the eutectic reaction to melt formation.

(2) B_4C powder and full SS pipe

To examine the eutectic melting between B_4C powder and SS, the powder is packed inside the SS tube with a packing ratio of 64%, as calculated by eq. (1).

$$packing\ ratio = \frac{\rho_{Bulk}}{\rho_{B_4C}} = \frac{M_{powder}}{V_{pow_{bulk}}\rho_{B_4C}} = \frac{M_{tube\ and\ powder} - M_{tube}}{\frac{\pi}{4} D_{tube}^2 L_{tube} \rho_{B_4C}} \quad (1)$$

where M is the mass (kg), V is the volume (m^3), L is the length (m), and ρ is the density (kg/m^3) of the respective subscripts. In the case of B_4C powder inside the SS full pipe, we observed the sintering of the powder when subjected to radiation heating. Sintering occurs due to solid-solid interactions between the B_4C particles at elevated temperatures. The B_4C particles agglomerate and fuse as the temperature rises, forming a solid mass. The sintering process is facilitated by the favorable contact area between the B_4C particles within the confined space of the SS pipe. Compared to the B_4C pellet case, the peeling-off of SS in the powder case is less smooth, as shown in Figure 7. This can be attributed to the denser packing of B_4C particles, which creates more significant resistance for the SS layer to peel off uniformly. In the B_4C powder case, the diffusion process between the individual B_4C powder particles and SS is relatively slow. The powder particles are separated by voids and spaces, not in direct contact.

Consequently, the available diffusion pathways are limited to the surface of the powder particles. The crystal structure of B_4C, covalently bonded and having a rigid and densely packed lattice, presents challenges for atoms to migrate across the interface, both in the pellet and powder case. But the weaker bonding between B_4C powder particles and SS and the limited contact area, results in a lower peeling-off of SS when compared the pellet case. The SS layer did not peel off entirely due to the weaker bonding and adhesive force. In our B_4C powder and SS experiments, we observed eutectic melt invasion. After the experiment, we noticed that the B_4C powder underwent sintering, resulting in a misshaped powder structure. This outcome occurred because the melt became trapped in the porous regions. However, with prolonged heating, we also observed movement and descent of the melt, which can be attributed to its low surface tension and viscosity at high temperatures. The melt form is again

settled at the bottom of the specimen like that of the pellet case. It's worth noting that Nagase et al. **[8]** also observed invasion in their B_4C powder and SS experiments. However, they did not observe the melt descent since their specimens were not subjected to long-term heating.

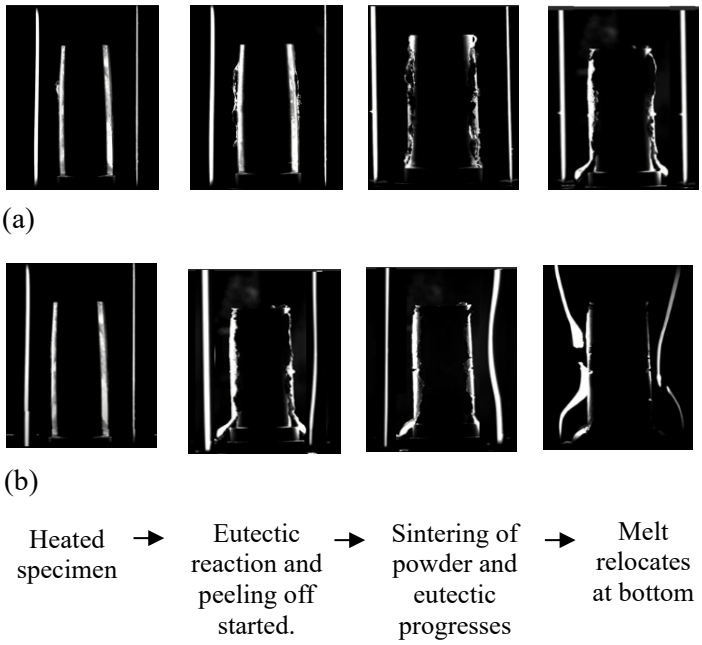

Fig. 7. (a) Experiment 1 and (b) Experiment 2 show the pictorial representation of the full SS pipe-powder case from the start of the eutectic reaction to melt formation.

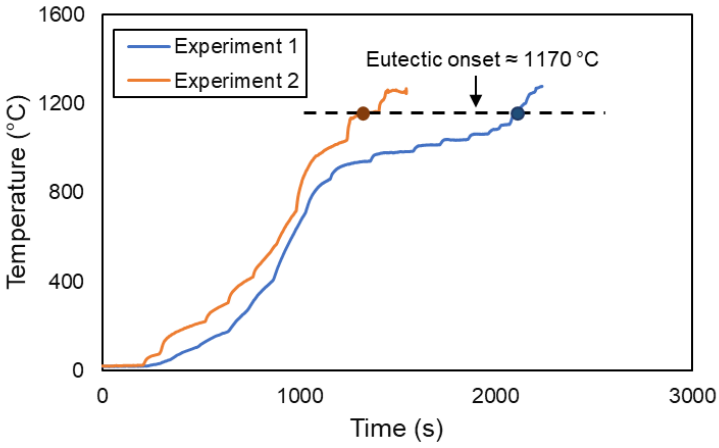

Fig. 8. Shows B_4C powder-Full SS pipe temperature profile with eutectic onset in two experiments with different heating rates.

Figure 8 shows the eutectic temperature in both experiments at different heating rates for the powder case. The melting occurs at a lower temperature of 1170 ºC. This is because the B_4C powder case shows better contact, and lower contact resistance, leading to an earlier eutectic melting temperature This is due to the eutectic liquid phase forming at a lower temperature, facilitated by enhanced atomic mobility and multiple interfaces facilitating interactions between B4C and SS. In contrast, the pellet case with imperfect contact experiences delayed formation of the eutectic liquid phase, resulting in a higher eutectic melting temperature. These findings align with previous studies conducted by **[8,17]**.

IV. Conclusions

This study utilized a quantitative and high-resolution visualization method using radiative heating to observe the eutectic behavior and resulting melt structure during boron migration. Experiments were conducted with B_4C pellets and powder within SS tubes, mimicking the actual control rod design, in the temperature range of 1150 °C to 1372 °C. This investigation provided unique insights into the long duration melting and relocation behavior, which had not been studied before. The study observed potential mechanisms that could occur inside the reactor under severe conditions. The eutectic temperature for the pellet case was higher than the powder case and was not influenced by the heating rate. Two failure mechanisms were identified: the SS peeling off the B_4C pellet and powder, forming a melting drop later, and the B_4C pellet breaking into multiple pieces possibly due to thermal stress, with sintering observed in the B_4C powder case. Additionally, the eutectic melting temperature was higher in the pellet case than in the powder case due to the loose initial contact and high contact resistance. Furthermore, the study effectively visualized the melt bead structure of real control rod geometry under high-temperature conditions, making it a potential dataset for validating numerical simulations. In future work, we will investigate the atomic mass percentage of the elements and the crystal structure present in the solidified eutectic melt. The current findings offer valuable insights into the relocation behavior of the eutectic melt, contributing to a better understanding of the eutectic reaction mechanism and eutectic melt progression in a damaged core. This study provides an important data set to refine existing models in severe accident codes for the safety assessment of CDAs in SFRs.

Acknowledgements

The present study is the result of "Technical development program on a common base for fast reactors" entrusted to the Japan Atomic Energy Agency (JAEA) by the Ministry of Economy, Trade and Industry (METI).

References

1. YAMANO, H., Kubo, S., Shimakawa, Y., Fujita, K., Suzuki, T. and Kurisaka, K., "Safety design and evaluation in a large-scale Japan sodium-cooled fast reactor," Science and Technology of Nuclear Installations (2012).
2. YAMANO, H., Takai, T., Furukawa, T., Kikuchi, S., Emura, Y., Kamiyama, K., ... and Nakamura, K., "Study on eutectic melting behavior of control rod materials in core disruptive accidents of sodium-cooled fast reactors:(1) project overview and progress until 2020," International Conference on Nuclear Engineering, vol. 85260, p. V003T12A008 (2021)
3. TOBITA, Y., Kamiyama, K., Tagami, H., Matsuba, K.I., Suzuki, T., Isozaki, M., Yamano, H., Morita, K., Guo, L. and Zhang, B., "Development of the evaluation methodology for the material relocation behavior in the core disruptive accident of sodium-cooled fast reactors," Journal of Nuclear Science and Technology, 53(5), pp.698-706 (2016).
4. SUZUKI, T., Kamiyama, K., Yamano, H., Kubo, S., Tobita, Y., Nakai, R. and Koyama, K., "A scenario of core disruptive accident for Japan sodium-cooled fast reactor to achieve in-vessel retention. Journal of Nuclear Science and Technology," 51(4), pp.493-513 (2014).
5. FUKAI, H., Furuya, M., and Yamano, H., "Raman spectroscopy of eutectic melting between boride granule and stainless steel for sodium-cooled fast reactors," Nuclear Engineering and Technology, 55(3), 902-907 (2023).
6. TAKANO, M., Nishi, T., and Shirasu, N., "Characterization of solidified melt among materials of UO_2 fuel and B_4C control blade," Journal of Nuclear Science and Technology, 51(7-8), 859-875 (2014).
7. HOFMANN, P. F., Markiewicz, M.E. and Spino, J.L., "Reaction behavior of B_4C absorber material with stainless steel and zircaloy in severe light water reactor accidents," Nuclear technology, 90(2), pp.226-244 (1990).
8. NAGASE, F., Uetsuka, H. and Otomo, T., "Chemical interactions between B_4C and stainless steel at high temperatures," Journal of nuclear materials, 245(1), pp.52-59 (1990).
9. SHIBATA, H., Sakamoto, K., Ouchi, A. and Kurata, M., "Chemical interaction between granular B_4C and 304L-type stainless steel materials used in BWRs in Japan," Journal of Nuclear Science and Technology, 52(10), pp.1313-1317 (2015).
10. SASAKI, R., Ueda, S., Kim, S-J., Gao, X. and Kitamura, S., "Reaction between B_4C and austenitic stainless steel in oxidizing atmosphere at temperatures below 1673 K," Journal of Nuclear Materials, vol. 466, pp. 334-342 (2015).
11. KOSTER, J-N., Derebail, R. and Grotzbach, A., "Visualization of convective solidification in a vertical layer of eutectic Ga-In melt," Applied Physics A, vol. 64, pp. 45-54 (1997).
12. KURETA, M., Kumada, H., Kume, E., Someya, S. and Okamoto K., "Dynamic neutron computer tomography technique for velocity measurement in liquid metal flow – Fundamental PTV experiment –," Journal of Physics: Conference Series, vol. 147, p. 012087 (2009)
13. TAKEDA, Y., "Development of an ultrasound velocity profile monitor," Nuclear Engineering and Design, vol. 126, pp. 277-284 (1991).
14. TASAKA, Y., Yanagisawa, T., Murai, Y. and Takeda, Y., "Ultrasonic visualization of fluid flow of liquid metal," Journal of the Visualization Society of Japan, vol. 26, pp. 252-257 (2006)
15. KOMIZO, Y., Terasaki, H., Yonemura, M. and Osuki, T., "In-situ observation of phase evolution in fusion welding of hypereutectoid carbon steel," Quarterly Journal of the Japan Welding Society, vol. 24, pp. 57-64 (2006).
16. SHINOZAKIi, K., Yamamoto, M., Wen, P. and Tamura, "M., Prediction of occurrence of solidification cracking in weld metal," Journal of the Japan Welding Society, vol. 77, pp. 284-289 (2008).
17. UEDA, S., Jo, B., Kondo, M., Erkan, N., Yajima, T. and Okamoto, K., "Initial relocation behavior of control rod materials in boiling water reactors studied via time-resolved visualization," Nuclear Engineering and Design, 333, pp.99-114 (2018).
18. YAMANO, H., Suzuki, T., Kamiyama, K., & Kudo, I., "Basic visualization experiments on eutectic reaction of boron carbide and stainless steel under sodium-cooled fast reactor conditions," International Atomic Energy Agency (2016)
19. HONG, Z., Pellegrini, M., Erkan, N., Liao, H., Yang, H., Yamano, H., and Okamoto, K., "A quantitative method of eutectic reaction study between boron carbide and stainless steel," Annals of Nuclear Energy, 180, 109462 (2023).
20. ABRAMOFF, M. D., Magalhães, P. J., and Ram, S. J., "Image processing with ImageJ." Biophotonics international, 11(7), 36-42 (2004).
21. TOMUT, M., Chiriac, H., Marinescu, M., and Necula, F., "Viscosity and surface tension measurements on Fe-rich FeB liquid alloys," Journal of non-crystalline solids, 250, 655-659 (1999).